Case History

Investigation of links between Precambrian basement structure and Paleozoic strata in the Fort Worth basin, Texas, U.S.A., using high-resolution aeromagnetic (HRAM) data and seismic attributes

Olubunmi O. Elebiju[1], G. Randy Keller[1], and Kurt J. Marfurt[1]

ABSTRACT

Effective hydraulic fracturing is critical for generating permeability within the Barnett Shale of the Fort Worth basin (FWB). Therefore, knowledge of the nature of the induced and natural fractures, faults, and collapse features that may form conduits to the underlying Ellenburger aquifer is vital. We use coherence and curvature seismic attributes, which are sensitive to faults, fractures, and collapse features, to map sedimentary features. We then integrate high-resolution aeromagnetic (HRAM) data with the seismic attributes extracted along the Ellenburger Formation and the top of basement from the north-central portion of the FWB, thereby linking features in the Precambrian basement to shallower sedimentary structures. HRAM-derived maps, designed to enhance basement structures, confirm that much of the sedimentary faulting is basement controlled. Specifically, attribute lineaments are aligned parallel to HRAM anomaly lineaments, consistent with regional tectonics. The northeast-southwest and northwest-southeast orientations of folds and faults in the sedimentary section parallel the northeast-trending Ouachita orogenic belt and the northwest-trending Muenster arch, which in turn correlate with reactivated Cambrian/late Precambrian basement faults. Mapping such features can aid in the design of the hydraulic fracture program and ability to predict structurally deformed areas of the basin.

INTRODUCTION

Almost all hydrocarbon production from the Barnett Shale of the Fort Worth basin (FWB) (Figure 1) requires inducing fractures while avoiding natural fractures, faults, and karst collapse features that form conduits to the underlying Ellenburger aquifer. The natural fractures tend to trend northwest and are thus subparallel to the Muenster arch, a reactivated older basement fault. The present-day northeast-trending stress field and induced fractures tend to parallel the northeast-trending Ouachita thrust front (Simon, 2005). Efforts by Montgomery et al. (2005), Sullivan et al. (2006), Aktepe et al. (2008), and Elebiju et al. (2008) suggest that Precambrian basement structures may be controlling some of the overlying Paleozoic features, such as faulting and karsting of the Ellenburger Formation and infill by the overlying Barnett Shale.

The existence of links between basement structure, hydrocarbon occurrences, and structures within the sedimentary section is not a new concept (e.g., Wilson and Berendsen, 1998; Plotnikova, 2006; Berger et al., 2008). Such relationships can be seen in the Paradox, Hardeman, Anadarko, Arkoma, Ardmore (Thomas and Baars, 1992), and Williston basins, among others (Gerhard and Anderson, 1988). However, using conventional seismic methods to establish such links is not trivial because basement structures may be difficult or expensive to delineate using seismic methods.

Our objective is to investigate the use of high-resolution aeromagnetic (HRAM) data to augment seismic images of basement and sedimentary structures within the north-central part of the FWB. We also explore the links and interactions between basement and sedimentary structures as well as how HRAM data can cost-effectively extrapolate seismic and drilling results into nearby regions without such control. We begin by reviewing HRAM methods and their use in studying basement features. Next, we review the tectonic setting of the FWB. After that, we present our methodology of linking HRAM anomalies to seismic attributes. This methodology includes enhancement and filtering techniques applied to HRAM data to highlight anomalies of potential interest not directly seen in the original data but caused by geologic features of interest. Using this meth-

odology, we develop an integrated magnetic and seismic interpretation of the area. We conclude by discussing advantages and pitfalls of our method.

HRAM DATA AND PRECAMBRIAN BASEMENT

The aeromagnetic method has long been recognized as an effective tool for mapping structures within Precambrian basement rocks where measured magnetic anomalies usually indicate magnetic susceptibility contrasts within the crystalline basement. HRAM data typically are acquired at flight heights closer to the ground (125–150 m) and with closer flight line spacing than traditional aeromagnetic surveys. Flight-line spacing for an HRAM survey can range from 200 to 800 m with a tie-line spacing of 600–2400 m, achieving an accuracy of approximately 0.1 nT (Berger et al., 2008; Peirce et al., 1998). Consequently, HRAM data improve the capability of mapping basement structures.

Applications of HRAM surveys in hydrocarbon exploration have increased because of the development of magnetometers that are more accurate, improved aircraft positioning using highly precise global positioning systems (GPS), and advances in data processing (Glenn and Badgery 1998; Peirce et al., 1998; Spaid-Reitz and Eick,
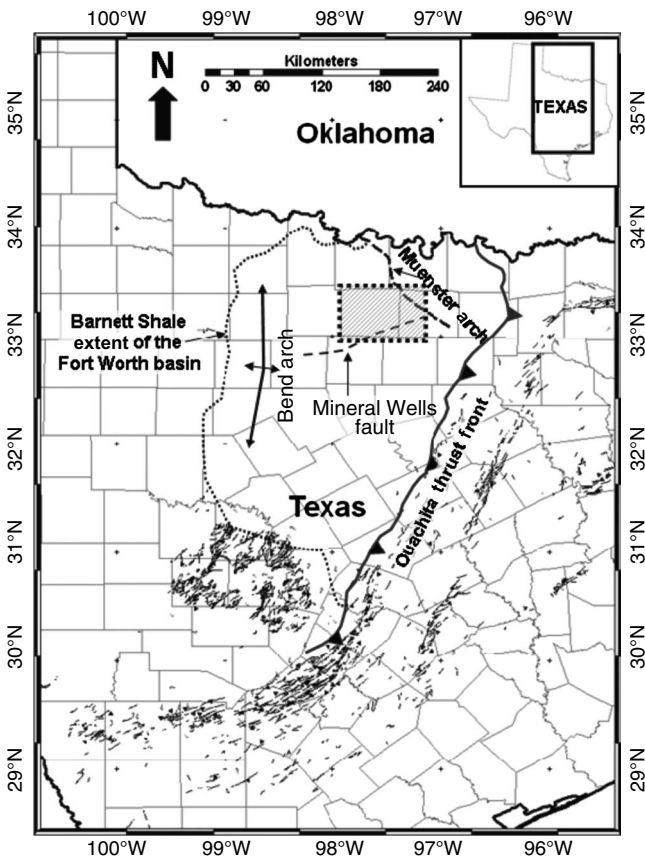

Figure 1. Map showing the Fort Worth basin province and major surrounding structural features: the Mineral Wells fault, Bend arch, the Ouachita thrust front, and the Muenster arch. The shaded rectangle shows the location of the seismic and HRAM data used in this study. (Map adapted from Pollastro et al., 2007. Mineral Wells fault adapted from Montgomery et al., 2005).

1998). Such improvements can be seen in applications to basement structure mapping (Gibson and Millegan, 1998) and intrasedimentary structure mapping (Grauch et al., 2001; Berger et al., 2008).

Algorithmic advances in extracting detailed information from magnetic data also have gained wide acceptance (e.g., Grauch and Cordell, 1987; Verduzco et al., 2004; Nabighian et al., 2005; Salem et al., 2007). Modern processing techniques for aeromagnetic data produce a variety of derivative or enhancement maps (e.g., tilt derivative and gradients) that extract important details from the data. Interpretation of magnetic data is nonunique, so interpreting HRAM data calls for an approach that integrates calibration with drilling, gravity, and/or seismic data.

Integrated approaches have been used in the FWB to establish a link between Precambrian basement structures and sedimentary basin structures and features (Elebiju et al., 2008). Other areas where such links have been established include Jonah field in the Green River basin, the Doig Sand play in the Horn River basin, and the Bakken play from the Williston basin in Canada (Stone, 2008). Jonah field consists of an unconventional basin-centered gas accumulation structurally controlled by a major northeast-trending basement-controlled wrench system. The Doig play develops along the downthrown side of the basement fault around an uplifted basement block. The crosscutting and offsetting of the Buick Creek basement block by basement faulting during reactivation controls the development and distribution of the Doig Sand play or sweet spots (Berger et al., 2008). Preferred trends of sedimentary structural traps that are largely controlled by basement structures difficult to detect from seismic or well-log data alone constitute the Bakken play.

HRAM surveys gradually are becoming a tool of choice for imaging subtle, deep Precambrian and shallow sedimentary structures. In the aforementioned basins, the HRAM data and its derivatives were used to image shallow structures and basement trends undetectable by the seismic data. HRAM also has been used to extend interpretations beyond the limits of existing seismic data coverage. We believe this approach can positively impact how basin-scale unconventional plays are mapped and exploited.

GENERAL TECTONIC SETTING OF STUDY AREA

The FWB is one of the major late Paleozoic foreland basins associated with the Ouachita orogenic belt, located along the southern margin of North America. The asymmetric basin's structural axis is aligned parallel to the east-bounding and advancing Ouachita structural front. The FWB is bounded on the west by the Bend arch, to the south by the Llano uplift, and to the north and northwest by basement uplifts of the Muenster and Red River arches, which were created by the reactivation of southern Oklahoma aulacogen basement faults during the Ouachita orogeny (Figure 1) (Walper, 1982; Keller et al., 1989). This classic failed rift intersects the early Paleozoic passive continental margin, which was stable until Mississippian time when the Ouachita orogeny began (e.g., Thomas, 1989).

Prior to the late Paleozoic orogeny that affected the FWB, the Grenville orogeny and Cambrian rifting affected the basement upon which the basin is deposited (Mosher, 1998). However, the Ouachita orogeny controlled the sedimentary history and structural setting of the FWB. The subsidence and sedimentation from the uplifted Ouachita thrust belt resulted in a westward migration of the depocenter with time and the development of the northeast-trending faulted an-

ticlinal flexure across the Llano uplift (Walper, 1982). These northeast-trending features disappear to the northeast, where the FWB intersects the Muenster arch. Deepening northward, the deepest part of the basin is located at its northeast corner adjacent to the Muenster arch, where the sediment thickness reaches about 3700 m (Montgomery et al., 2005).

In the FWB region, late Paleozoic-Mississippian movements periodically reactivated a northeast–southwest-trending Precambrian structure that was mapped across the Newark East field. This structure, termed the Mineral Wells fault, is important to exploration within the FWB because it controls sediment deposition as well as oil and gas distribution. Specifically, it prohibits gas accumulation in the Barnett Shale within the Newark East field, where it intercepts closed fractures (Figure 1). Other minor structures subparallel to the Mineral Wells fault and the Ouachita thrust front have been identified by Montgomery et al. (2005).

METHODOLOGY

The integrated geophysical methodology used in this study consists of 3D seismic data analysis supplemented by HRAM data analysis. Figures 1 and 2 show the location of the HRAM and 3D seismic data used for the study. Within the FWB, we hypothesize that calibrating HRAM derivative images and HRAM Euler deconvolution results with scattered 3D seismic surveys can provide a means to accurately map and study the relationships between the basement structures and the overlying sedimentary structures in areas where seismic data are unavailable.

HRAM and seismic data

Devon Energy, as part of its Barnett Shale exploitation program, contracted the acquisition and processing of the seismic data used for this study. Airmag Surveys Inc. acquired the HRAM data on behalf of Mitchell Energy (Devon's predecessor) during January and February 2000. The HRAM survey was flown at 152 m ground clearance, with an east-west profile separation of 402 m tied by north-south lines spaced at 805 m. A total of 31,000 line-kilometers constituted the mileage for the two areas.

Corrections applied to the HRAM data by Pearson, deRidder, and Johnson Inc. included removing the international geomagnetic reference field (IGRF), leveling, and adjusting for diurnal changes. Cultural noise was removed, and the data were interpolated to a 100-m grid.

Seismic data

Conventional work flows for most seismic interpreters involve integrating seismic data, well logs, production data, and geologic outcrop data. Although seismic data can be areally extensive in terms of its denser coverage, it is often plagued with lower vertical resolution. On the other hand, production data, well logs, and geologic outcrop data have a higher vertical resolution but are areally limited or restricted. The seismic survey was designed and prestack time-migrated to accurately map the relatively flat-lying target horizons in the sedimentary column. However, mapping below the Ellenburger unconformity and into the Precambrian basement requires prestack depth migration (Aktepe et al., 2008). Furthermore, very few wells penetrate the Precambrian basement within the survey area.

Using seismic data and seismic attributes, we adopted a conventional seismic interpretation workflow for mapping structures. The seismic attributes were generated in house, and we extracted the desired attributes along the Ellenburger horizons and the top of basement. The coherence and the most negative curvature attributes were very useful. Hakami et al. (2004), Sullivan et al. (2006), and Aktepe et al. (2008) effectively use these kinds of attributes to study the sedimentary features within the FWB. The physical and geometric features in these attributes use models or seismic characteristics of dip and azimuth, amplitude, phase, frequency content, and waveform similarity from adjacent seismic samples (Chopra and Marfurt, 2007).

Coherence is a measure of seismic waveform or trace similarity. This attribute is sensitive to lateral changes in the physical models or seismic characteristic mentioned above, and their lateral sensitivity makes them suitable to map features such as faults (Lawrence, 1998) and fractures (Neves et al., 2004) effectively.

Curvature is a measure of reflector folding. Every sample in the seismic survey is represented by a local dip and azimuth (e.g., Marfurt, 2006). For a 2D cylindrical surface, curvature is the reciprocal of the radius of a circle tangent to a surface. For 3D surfaces, we need to define two orthogonal circles whose radii define the principal curvatures k_1 and k_2 of a local surface. The most negative principal curvature k_2 is always less than or equal to the signed value of the most positive principal curvature k_1 (Mai et al., 2009). Bowls and valleys are represented by strongly negative k_2 values; domes and ridges are represented by strongly positive k_1 values. Curvature attributes facilitate the mapping of subtle folds and faults whose throw falls below seismic resolution (Blumentritt et al., 2006), karst-modified fractures (Nissen et al., 2008), and collapse features (Sullivan et al., 2006; Aktepe et al., 2008).

HRAM data and derivative maps

We regridded the HRAM data to 400-m grid spacing using a minimum-curvature algorithm available in a commercial gravity and magnetic processing and interpretation software package. This grid spacing is appropriate for selecting a window size for our Euler deconvolution depth estimation. The window size indicates the grid cell area used to compute the Euler solutions. The size of anomaly of interest and the grid size determine the window size. The window must be large enough to include the anomaly of interest but not multiple anomalies. Because we want to map anomalies of about 5 km wide and 3–5 km in depth, the grid spacing of 0.4 km requires a window of about 13 grid cells (Phillips, 2007).

Before any interpretation is done on the HRAM data, the data must be reduced to the pole (RTP) to remove magnetic anomaly distortion caused by varying magnetization inclination and azimuth (Kis, 1990). To highlight local anomalies, we generate an RTP residual total magnetic intensity (TMI) map (Figure 2a) by subtracting grid values calculated by upward continuing the original RTP HRAM data to 5 km (to represent regional anomalies; Figure 2b) from the original TMI HRAM grid. Maps for several upward-continuation heights (e.g., 1 km, 10 km, etc.) were generated and evaluated before we chose the height that we felt best represented the regional anomaly.

To highlight lateral or abrupt changes in magnetization that can suggest faults or source contacts, we computed the horizontal gradient magnitude (HGM), tilt derivative, and horizontal derivative of the tilt derivative from the HRAM data (Figure 3). These processes

are edge-detecting derivatives that enhance lateral discontinuities in a TMI grid (e.g., Grauch and Cordell, 1987; Roest et al., 1992; Blakely, 1996; Verduzco et al., 2004). In addition to source shape and edge detection, the horizontal derivative of the tilt derivative can effectively map shallow basement structures, delineating induced or remanent magnetized bodies with anomalies centered over the body edges (Verduzco et al., 2004). The interpreter still has the responsibility of providing a geologically meaningful interpretation of what is seen on these maps.
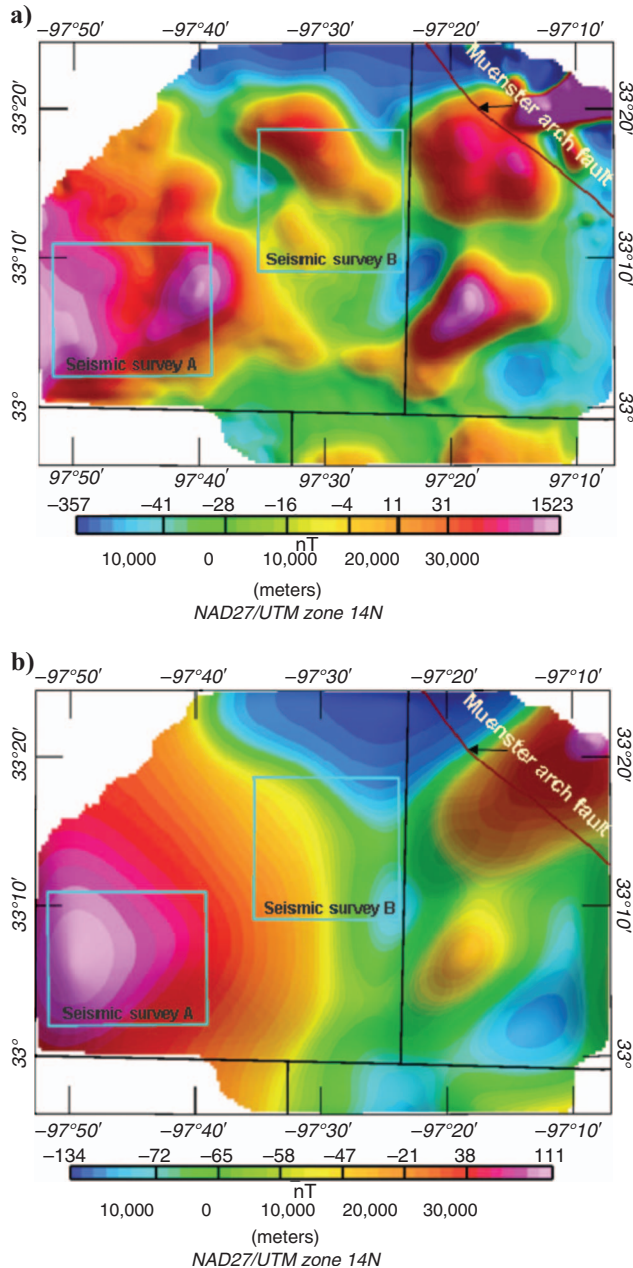

Figure 2. (a) RTP residual TMI map generated by subtracting the 5-km upward-continuation grid from the original TMI HRAM grid. Cyan boxes show the location of the two seismic data sets used for seismic interpretation and seismic attribute analysis. (b) Map showing the 5-km upward-continuation grid subtracted from the original TMI map to produce the RTP map in (a). Broad anomalies (indicated by warm colors) are related to deep regional features that mask the more local crustal features, enhanced on the residual RTP map.

Euler deconvolution (Thompson, 1982) estimates the location and upper and lower bounds on the depth of hypothesized dikes, faults, magnetic contacts, and extrusives (Phillips, 2007). The Euler deconvolution structural index N describes the geometry of the desired geologic structure (Reid et al., 1990; Barbosa et al., 1999). For each assumed shape (i.e., structural indices of 0.0, 0.5, and 1.0), the interpreter examines a suite of analysis window sizes that balances accuracy and lateral resolution (Phillips, 2007). The analysis window should be large enough to contain the curvature of the anomaly of interest without compromising lateral resolution, yet small enough to reduce interference from an adjacent anomaly that would yield poor results (Reid et al., 1990).

We display Euler deconvolution images for $N = 1$ (delineating small-vertical-offset faults; Figure 4a) and $N = 0$ (delineating larger vertical-offset faults; Figure 4b). Only solutions with less than 25% error are plotted. Following Reid (1990), we used the HRAM data (without RTP) to estimate the magnetic anomaly source type and fault trend at the top of the Precambrian basement as well as to estimate the overlying sediment thickness (Li, 2003).

INTEGRATED ANALYSIS AND INTEGRATED INTERPRETATION

Area of seismic survey A

Our integrated analysis and interpretation were based on areas where seismic and HRAM data are available (Figure 2). In seismic survey A, a coherence time slice extracted along the Ellenburger shows major faults F_1-F_1', F_2-F_2', and F_3-F_3' (Figure 5a). The faults that trend east-west and northeast-southwest agree with interpretations by Sullivan et al. (2006); in fact, some of our seismic interpretation conclusions are extracted from their work. Sullivan et al. (2006) interpret a wrench (normal) fault (F_2-F_2' and F_3-F_3' on Figure 5a) and antithetic strike-slip faults (F_1-F_1' on Figure 5a) that penetrate the Precambrian basement.

Circular to elliptical collapse features, which appear as low-coherence fingerprints on the coherence image (Figure 5a), also have a strong bowl shape (Figure 5c). Many of these collapse features are aligned along northeast and northwest orientation (Figure 5a) and correlate with the intersection of the valley-shaped lineaments (Figure 5a and c) that continue into the basement, suggesting basement control of the collapse features (Sullivan et al., 2006). Faults interpreted on the coherence time slice (Figure 5a) are also seen on the k_2 principal-curvature time slice (Figure 5b).

To compare structures seen within the sedimentary section via seismic attributes with Precambrian basement structures, we generated a series of Euler deconvolution plots and derivative magnetic maps (Figure 6). Within the area occupied by seismic survey A, the horizontal gradient magnitude (Figure 6a), the tilt derivative (Figure 6b), and the horizontal derivative of the tilt derivative (Figure 6c) anomaly maps generated from the HRAM data show a lineament trend parallel to the wrench fault interpreted from the seismic data. The maxima of the horizontal gradient magnitude and the horizontal derivative of the tilt-derivative grid and value close to zero on the tilt derivative indicate the magnetic-source shapes and edges. However, the east-west strike-slip fault interpreted on the seismic data cannot be identified on the derivative anomaly maps (Figures 5 and 6). This inability to image the strike-slip fault on the derivative maps suggests that the fault does not have sufficient vertical or lateral displacement to cause a magnetic-susceptibility contrast.
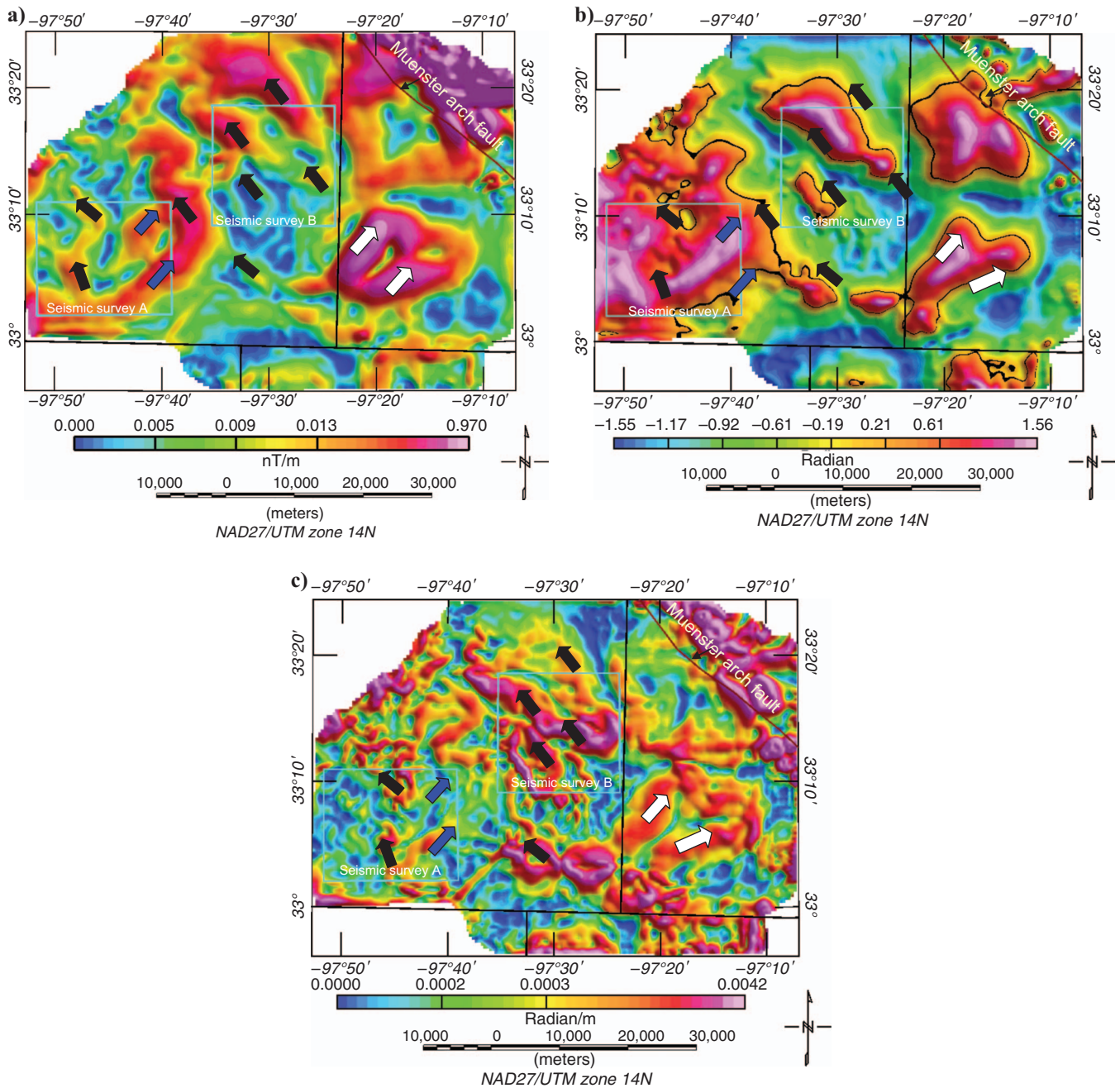
Figure 3. (a) Horizontal gradient magnitude (HGM), (b) tilt derivative, and (c) total horizontal derivative of the tilt derivative, computed from the TMI HRAM grid in Figure 2a. Maxima (e.g., horizontal gradient maxima and total horizontal derivative of the tilt derivative) and zero value (e.g., tilt derivative) are located at magnetic source edges. Black lines on (b) indicate the zero values of the tilt derivative. White arrows indicate the location of northeast-trending maxima where we predict a northeast-trending fault will be present within the sedimentary section. The blue and black arrows are additional northeast- and northwest-trending maxima, respectively. The Mineral Wells fault was interpreted to be present at this location based on seismic data (Perez et al., 2009).

Within the area of seismic survey A, we notice linear clustering of Euler depth solutions ($N = 1.0$) that trend northeast and northwest (Figure 6d). The northeast-trending lineaments indicated by the black arrow close to $F_2-F_2{}'$ and $F_3-F_3{}'$ are parallel with the northeast regional wrench fault identified on the seismic attribute data (Figure 5). The linear clusters represented by the blue and green circles suggest two source depths that correspond to between 3 and 6 km, which in turn correlate to a seismic depth of basement of 3 km. The crystalline Precambrian basement is suggested to be the magnetic source.
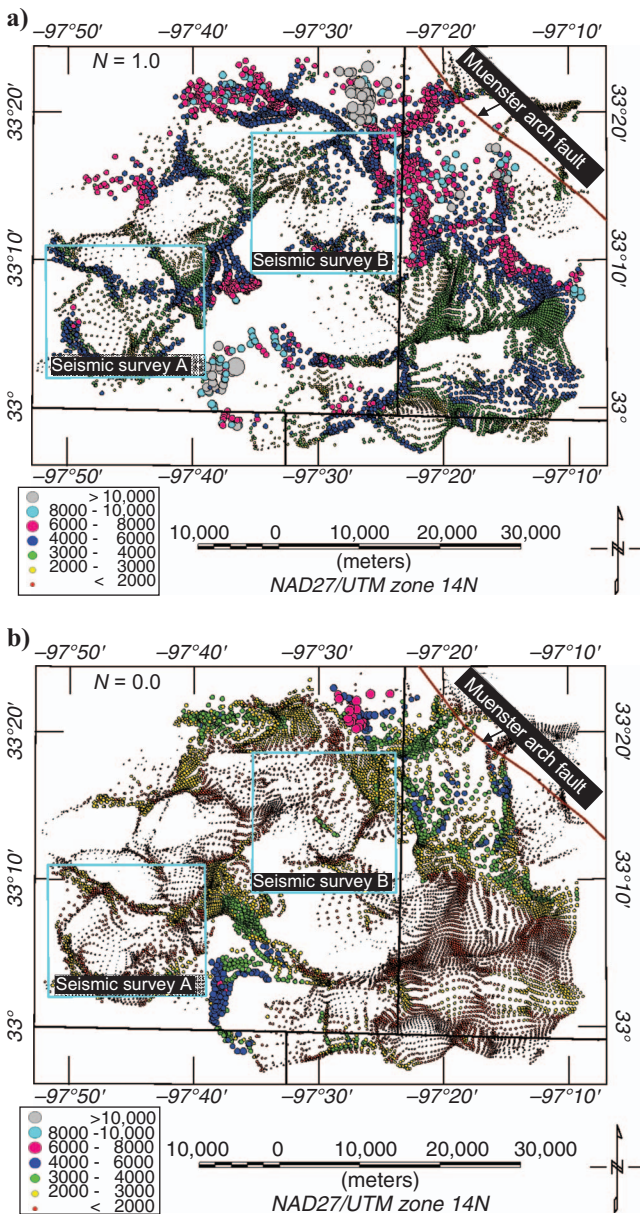
The lateral offset of the deeper magnetic anomalies (black arrows, Figure 6d) from the shallower regional wrench fault interpreted on seismic data suggests that the fault dips to the northwest within the basement. Other linear clusters located in the southwest corner and upper half of seismic survey A area do not correlate with any seismic lineaments. However, they terminate against the east-west seismic lineament interpreted as an antithetic strike-slip fault (Sullivan et al., 2006).

In an independent study (Perez et al., 2009), a strike-slip fault located 25 km east and southeast of seismic surveys A and B, respectively, was found to run parallel to another northeast-trending derivative anomaly lineament, indicated by northeast-trending white arrows in Figure 3. Based on our work flow, we predict that a northeast-trending fault will be present within the sedimentary section above these anomalies. Although the seismic data for that location were not available for this study, a northeast-trending basement penetrating the sedimentary Mineral Wells fault (Montgomery et al., 2005) has been interpreted on seismic data at this location (Perez et al., 2009). Thus, our interpretation further suggests that HRAM data can be used to predict sedimentary features where seismic data are unavailable or limited.

Area of seismic survey B

Seismic survey B (Figure 7) shows more diverse lineament orientations than survey A. On the coherence and k_2 time slices extracted along the top of the Ellenburger Formation, we identified three lineaments: two orthogonal lineaments trend northeast ($F_4-F_4{}'$) and northwest ($F_6-F_6{}'$) and one lineament trends east–west ($F_5-F_5{}'$) (Figure 7). On similar attributes extracted near the top of basement, we also observed trends of lineaments similar to what was described near the top of the Ellenburger Formation. These lineaments appear on the time slices shown in Figure 7c and d. Because of the limits of time migration below the high-velocity Ellenburger Formation, the seismic data quality becomes more incoherent as we approach basement (Figure 7). Nonetheless, lineaments interpreted from the top of the Ellenburger Formation can be extrapolated on the coherence and k_2 time slices extracted near the top of basement.

Evaluation and comparison of aeromagnetic anomaly trends seen on the horizontal gradient magnitude map (Figure 8a), tilt derivative (Figure 8b), and horizontal derivative of the tilt derivative (Figure 8c) with lineament trends from seismic interpretation and Euler depth plot (Figure 8d) reveal similarities in the azimuths of the lineaments on these maps. From the Euler depth plot, we could identify three lineament trends that are not easily distinguishable on the derivative maps. We interpret the lineaments seen on the attribute data as faults. These faults, which trend northeast, northwest, and east-west, parallel anomaly trends seen on the horizontal derivative of the tilt-derivative map. Similarly, the linear clustering of some of the Euler depth solutions is parallel to these faults (Figure 8d).

Borehole information within the study area shows healed fractures to exhibit trends synonymous with these lineaments (Rich, 2008). Simon (2005) also uses borehole breakout measurements from image logs to identify fractures that trend northeast. In those

Figure 4. Euler deconvolution cluster plots computed using structural indices of (a) $N = 1.0$, appropriate for delineating low-displacement faults, and (b) $N = 0.0$, appropriate for delineating large displacement faults.

wells with image logs, the maximum horizontal stress estimated by velocity anisotropy and the hydraulic fractures examined using microseismic data propagate predominantly northeast. In other, more isotropic areas, the hydraulic fractures form a relatively uniform northeast-northwest trend.

These similarities in orientation between sedimentary and Precambrian basement structures are common to both survey areas studied (Figures 6d and 8d). Although the anomalies from the Precambrian basement are not coincidental with sedimentary features, they are coupled. We interpret the northeast-trending features in Figure 6b to be basement-penetrating faults with a northwest dip. In Figure 8d, we observe southeast and northeast dipping of the northeast- and northwest-trending basement penetrating faults, respectively. Because of the close proximity of these structures to the northeast-trending Ouachita thrust front, we expect a preponderance of south-dipping structures. Nonetheless, the presence of northwest- and southeast-dipping features is not surprising. The Ouachita thrust system has a limited exposure but widespread effect within the FWB (Keller et al., 1989). According to Harry and Londono (2004), the thin-skinned (nonbasement involved) and thick-skinned (basement involved) thrusting of the Ouachita thrust system share common along-strike structural changes. The southeast-dipping, thick-skinned thrust systems are common within the Ouachita system. However, near the southern edge of the system, north-dipping, thin-skinned systems are emplaced (Harry and Londono, 2004).

Some structures and deposits found within the FWB are controlled by the northwest-directed Ouachita orogenic compression. In a remotely sensed surface lineament study conducted east of the FWB near the Ouachita thrust front subcrop, northeast faults and surface lineaments documented from Landsat images were subparallel to the Ouachita basement structural fabric (Caran et al., 1981). In addition, northeast-trending normal faults and anticlinal flexures of Atokan age that offset the basement developed across the exposed Llano uplift to the south of the FWB. These northeast-trending features disappear to the northeast toward the Muenster arch (Ewing, 1991).

In contrast, the natural fractures have orientations parallel to the northwest-trending lineaments that are parallel to the Muenster arch, a reactivated basement fault. Preexisting basement faults associated with the formation of the Cambrian-rifted southern edge of the North American craton may be related to the Muenster arch and the Ouachita thrust (Hale-Erlich and Coleman, 1993).

Faults within the sedimentary section often indicate basement reactivation. Locally, sedimentary zones of weakness follow those that existed within the basement rocks. On a regional scale, strains generally are related to deep crustal movements during reactivation and may be directly expressed as faults and shear zones in the overlying sedimentary cover (Jacques, 2003).

We therefore interpret the HRAM lineaments within the study area as zones of weakness within the basement. The lineaments in the seismic illuminated sedimentary section are interpreted as a product of basement reactivation and surface expression of potential zones of weakness within the basement. The lateral offset of the shallower sedimentary features from the deeper basement features is the result of dip associated with fault planes of faults that extend down into the Precambrian basement.
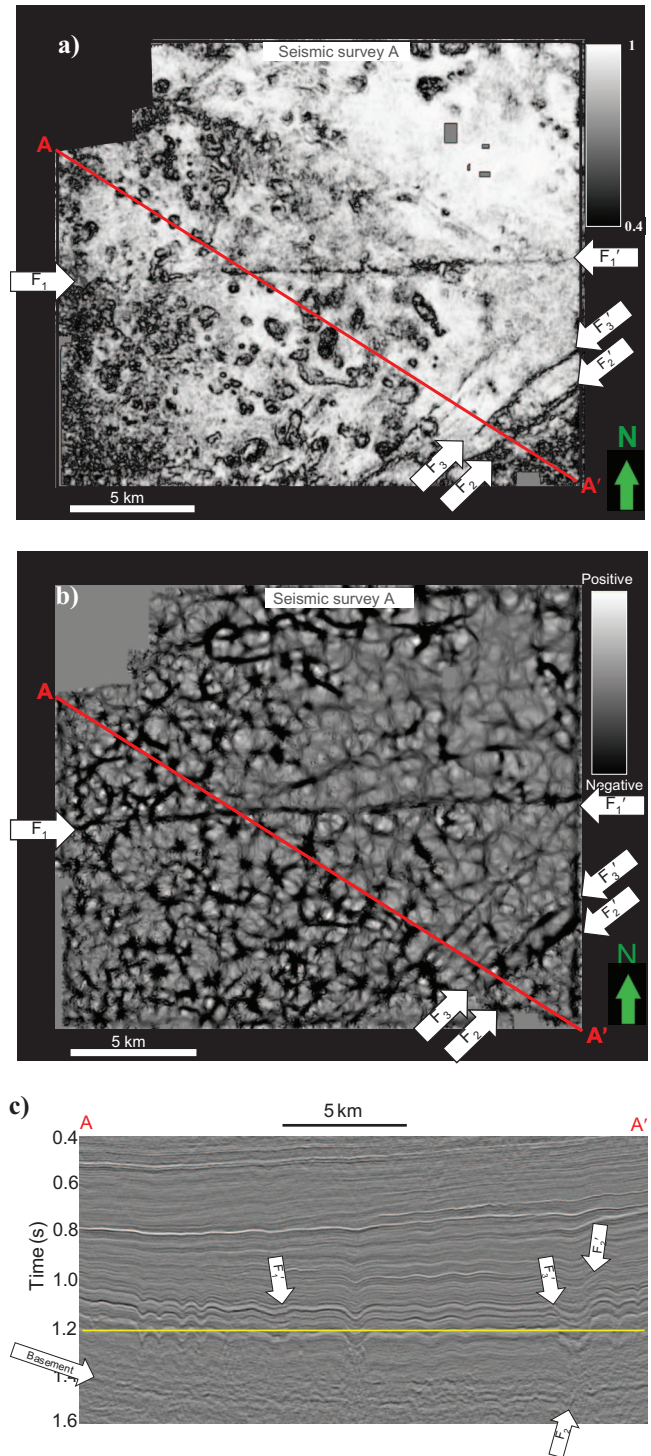

Figure 5. Ellenburger time slices (at approximately 1.2 s) through (a) coherence and (b) k_2 most-negative principal curvature time slices, computed from seismic survey A. Line A−A′ is shown on (c). Fault F_1−F_1′ is an east-west strike-slip fault; faults F_2−F_2′ and F_3−F_3′ are normal faults consistent with the interpretation of Hakami et al. (2004) and Sullivan et al. (2006). Low-coherence elliptical anomalies correlate to collapse features. (c) Vertical slice A−A′ through the seismic amplitude volume, showing the strike-slip fault F_1−F_1′ and two of the larger normal faults, F_2−F_2′ and F_3−F_3′ that propagate into the basement. The yellow line indicates the time slice shown on the previous figures. Note the series of collapse features.
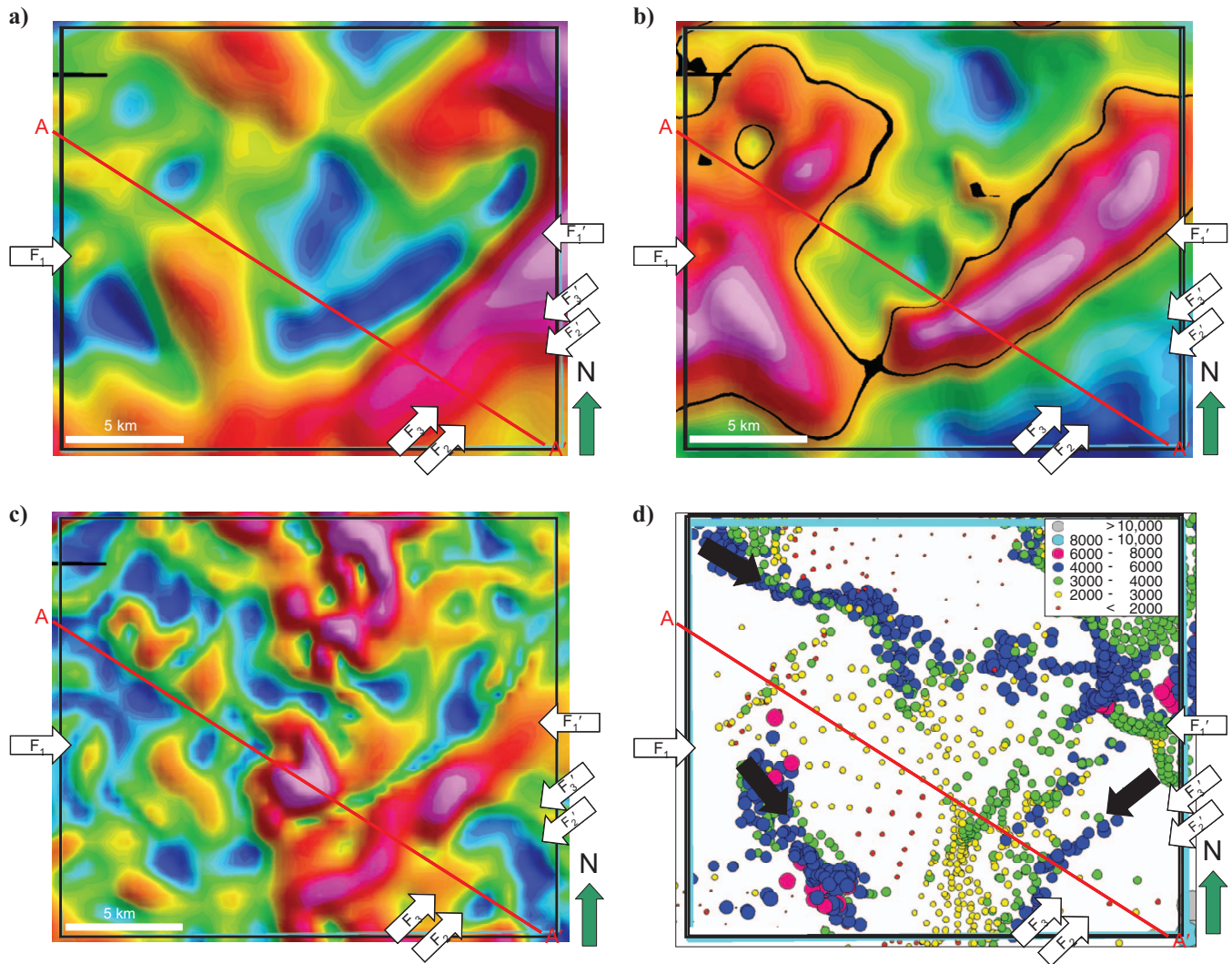
Figure 6. The (a) horizontal gradient magnitude, (b) tilt derivative, (c) horizontal derivative of the tilt derivative, and (d) Euler deconvolution cluster plot with $N = 1.0$ for the area of seismic survey A. Lineaments $F_1 - F_1'$, $F_2 - F_2'$, and $F_3 - F_3'$ are the sedimentary faults interpreted on seismic data. Black arrows on (d) are lineament trend interpretations from the Euler plot. The northeast-trending normal fault $F_1 - F_1'$ appears to be parallel to a linear trend (black arrow) from the Euler deconvolution estimation, which reflects basement structures. These linear clusters suggest that the source body dips to the northwest.
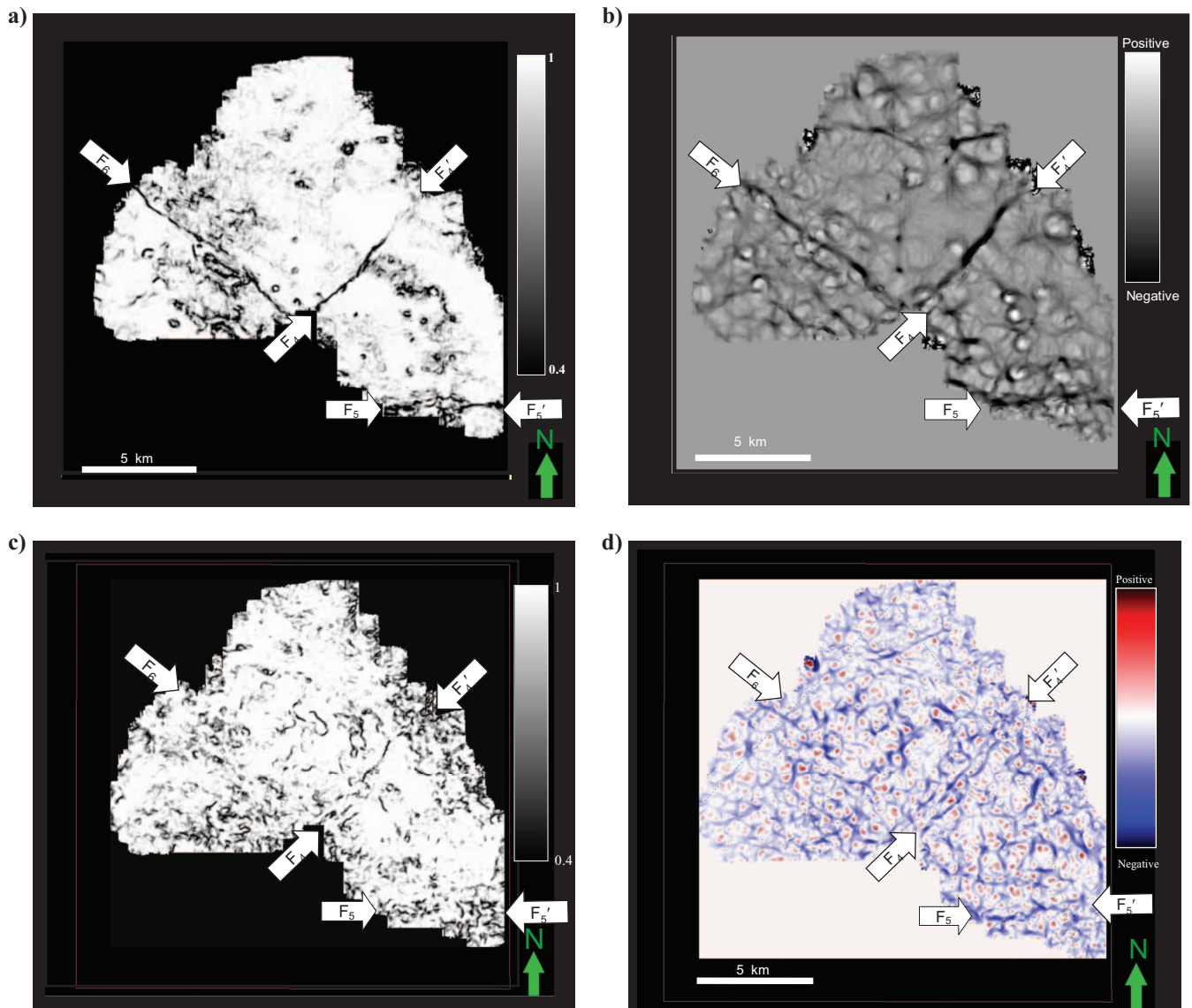
Figure 7. Ellenburger time slices (at approximately 1.34 s) through (a) coherence and (b) k_2 most-negative principal curvature time slice, computed from seismic survey B. Time slices near the top of basement (at approximately 1.8 s) through (c) coherence and (d) most-negative curvature horizon slice, computed from seismic survey B. The F_5–F_5' (east-west), F_4–F_4' (northeast), and F_6–F_6' (northwest) lineaments are the major faults interpreted. Intrasedimentary structures interpreted on the Ellenburger Formation appear to penetrate the Precambrian basement.
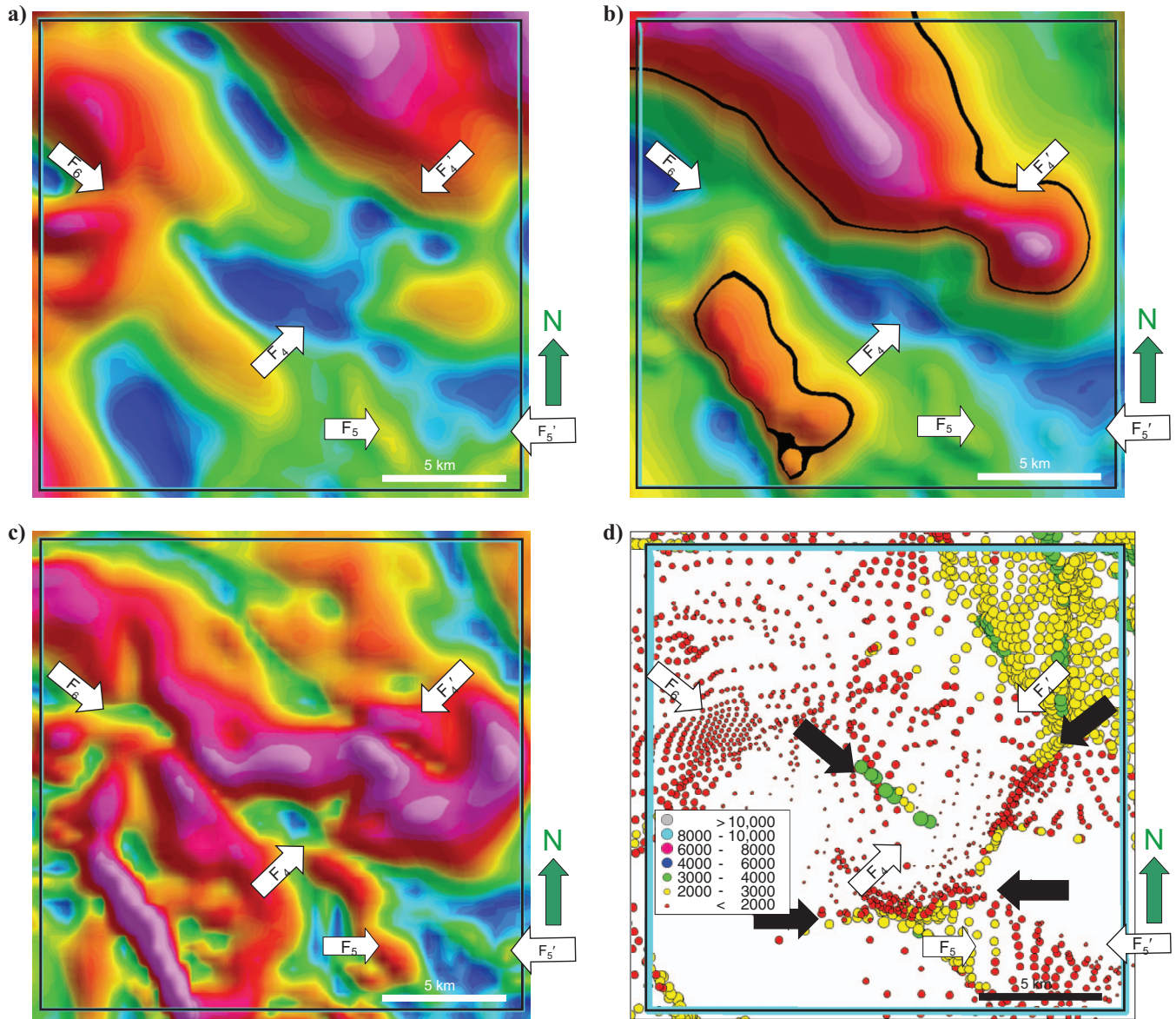
Figure 8. The (a) horizontal gradient magnitude, (b) tilt derivative, (c) horizontal derivative of the tilt derivative, and (d) Euler deconvolution cluster plot with $N = 0$ for seismic survey B. Lineaments F_4-F_4', F_5-F_5', and F_6-F_6' are the location of sedimentary faults interpreted on seismic data. Black arrows on (d) are lineament trends interpreted from the Euler plot. The clusters of lineaments from the Euler plot appear offset to the seismic interpreted features. The northeast, northwest, and east-west faults appear parallel to linear trends from the Euler deconvolution depth estimation that follow basement structures.

CONCLUSIONS

The orientation of faults and collapse features mapped using seismic attributes are parallel to trends mapped using HRAM data in the FWB. The northeast-southwest and northwest-southeast orientation of these features are consistently parallel with Precambrian structural fabric that forms large-scale structures such as the northeast-trending Ouachita orogenic belt and the northwest-trending Muenster arch. We interpret the propagation of the Precambrian structural fabric through the sedimentary section along zones of weakness as responsible for creating the linear faults and joints in the Paleozoic section. The resulting dip associated with the fault plane is responsible for the lateral offset seen between the sedimentary features seen on the seismic attribute data and aeromagnetic lineaments

Calibrating nonunique, large-scale, lower-resolution, less-expensive HRAM data with moderate-scale, higher-resolution, expensive seismic data enhances our prediction of interaction between basement structures and sedimentary structures where seismic data are unavailable or limited. Based on our analysis of the HRAM data, we predict the occurrence of the northeast fault systems beneath the Mineral Wells fault, where seismic data are absent, and confirm this prediction with an independent seismic study.

Although dozens of 3D seismic surveys cover the FWB, basin-scale shale reservoirs are being developed throughout North America as well as in eastern Europe and southern Africa. We believe our methodology will be useful in mapping basement structures that, coupled with an appropriate geologic model, can help identify locations for more expensive 3D seismic surveys. In frontiers areas where seismic data are limited, HRAM data can be used inexpensively to determine the lateral extent of structures interpreted on seismic data. HRAM data are also faster to acquire than seismic data, significantly reducing exploration cycle time.

Our results show that the integration of derivative images from high-resolution aeromagnetic data with scattered 3D seismic surveys can provide a means of effectively mapping basement features and establishing a link between the basement and sedimentary structures within the north-central part of the FWB. The knowledge gained will positively influence oil and gas exploration and development within the study area because the orientation of natural fractures can be predicted even if seismic data are limited or unavailable. Mapping such features can aid in designing the hydraulic fracture program and predicting areas of the basin that may be more structurally deformed.

REFERENCES

Aktepe, S., K. J. Marfurt, and R. Perez, 2008, Attribute expression of basement faulting — Time versus depth migration: The Leading Edge, **27**, 360–367.

Barbosa, V. C. F., J. B. C. Silva, and W. E. Medeiros, 1999, Stability analysis and improvement of structural index estimation in Euler deconvolution: Geophysics, **64**, 48–60.

Berger, Z., M. Boast, and M. Mushayandebvu, 2008, The contribution of integrated HRAM studies to exploration and exploitation of unconventional plays in North America: Reservoir, **35**, 42–48.

Blakely, R. J., 1996, Potential theory in gravity and magnetic applications: Cambridge University Press.

Blumentritt, C. H., K. J. Marfurt, and E. C. Sullivan, 2006, Volume-based curvature computations illuminate fracture orientations — Early to mid-Paleozoic, Central Basin Platform, west Texas: Geophysics, **71**, no. 5, B159–B166.

Caran, S. C., C. M. Woodruff, and E. J. Thompson, 1981, Lineament analysis and inference of geologic structure — Examples from the Balcones/Ouachita trend of Texas: Transactions, Gulf Coast Association of Geological Societies, **31**, 59–69.

Chopra, S., and K. J. Marfurt, 2007, Seismic attributes for prospect identification and reservoir characterization: SEG.

Elebiju, O. O., G. R. Keller, and K. J. Marfurt, 2008, New structural mapping of basement features in Fort Worth basin, Texas, using high-resolution aeromagnetic derivatives and Euler depth estimates: 78th Annual International Meeting, SEG, Expanded Abstracts, 844–848.

Ewing, T. E., 1991, The tectonic framework of Texas, *in* W. L. Fisher, ed., Text to accompany "The Tectonic Map of Texas:" Bureau of Economic Geology, The University of Texas at Austin, scale 1:750,000.

Gerhard, L. C., and S. B. Anderson, 1988, Geology of the Williston basin (United States portion), *in* L. L. Sloss, ed., Sedimentary cover — North American Craton, U.S.: Geological Society of America, vol. D-2, 221–241.

Gibson, R. I., and P. S. Millegan, 1998, Geologic applications of gravity and magnetics: Case history: SEG Geophysical References Series No. 8.

Glenn, W. E., and R. A. Badgery, 1998, High resolution aeromagnetic surveys for hydrocarbon exploration: Prospect scale interpretation: Canadian Journal of Exploration Geophysics, **34**, 97–102.

Grauch, V. J. S., and L. Cordell, 1987, Limitation of determining density or magnetic boundaries from the horizontal gradient of gravity or pseudogravity data: Geophysics, **52**, 118–121.

Grauch, V. J. S., M. R. Hudson, and S. A. Minor, 2001, Aeromagnetic expression of faults that offset basin fill, Albuquerque basin, New Mexico: Geophysics, **66**, 707–720.

Hakami, A. M., K. J. Marfurt, and S. Al-Dossary, 2004, Curvature attributes and seismic interpretation: Case study from Fort Worth Basin, Texas, USA: 74th Annual International Meeting, SEG, Expanded Abstracts, 554–547.

Hale-Erlich, W. S., and J. L. Coleman, 1993, Ouachita-Appalachian juncture: A Paleozoic transpressional zone in the southeastern USA: AAPG Bulletin, **77**, 552–568.

Harry, D. L., and J. Londono, 2004, Structure and evolution of the central Gulf of Mexico continental margin and coastal plain, southeast United States: Geological Society of America Bulletin, **116**, 188–199.

Jacques, J. M., 2003, A tectonostratigraphic synthesis of the sub-Andean basins: Implications for the geotectonic segmentation of the Andean Belt: Journal of the Geological Society of London, **160**, 687–701.

Keller, G. R., J. M. Kruger, K. J. Smith, and W. M. Voight, 1989, The Ouachita system: A geophysical overview, *in* R. D. Hatcher, W. A. Thomas, and G. W. Viele, eds., The Appalachian-Ouachita orogeny in the United States: Geological Society of America, 689–694.

Kis, K. I., 1990, Transfer properties of the reduction of magnetic anomalies to the pole and to the equator: Geophysics, **55**, 1141–1147.

Lawrence, P., 1998, Seismic attributes in the characterization of small-scale reservoir faults in Abqaid field: The Leading Edge, **17**, 521–525.

Li, X., 2003, On the use of different methods for estimating magnetic depth: The Leading Edge, **22**, 1090–1099.

Mai, H. T., K. J. Marfurt, and S. Chavez-Perez, 2009, Coherence and volumetric curvature and their spatial relationship to faults and folds: An example from Chicontepec basin, Mexico: 79th Annual International Meeting, SEG, Expanded Abstracts, 1063–1067.

Marfurt, K. J., 2006, Robust estimates of 3D reflector dip: Geophysics, **71**, no. 5, 29–40.

Montgomery, S. L., D. M. Jarvie, K. A. Bowker, and R. M. Pollastro, 2005, Mississippian Barnett Shale, Fort Worth basin, north-central Texas: Gas shale play with multi-trillion cubic foot potential: AAPG Bulletin, **89**, 155–175.

Mosher, S., 1998, Tectonic evolution of the southern Laurentian Grenville orogenic belt: Geological Society of America Bulletin, **110**, 1357–1375.

Nabighian, M. N., V. J. S. Grauch, R. O. Hansen, T. R. LaFehr, Y. Li, J. W. Peirce, J. D. Phillips, and M. E. Ruder, 2005, The historical development of the magnetic method in exploration: Geophysics, **70**, no. 6, ND33–ND61.

Neves, F., M. S. Zahrani, and S. W. Bremkamp, 2004, Detection of potential fractures and small faults using seismic attributes: The Leading Edge, **23**, 903–908.

Nissen, S. E., T. R. Carr, K. J. Marfurt, and E. C. Sullivan, 2008, Using 3-D seismic volumetric curvature attributes to identify fracture trends in a de-

pleted Mississippian carbonate reservoir: Implications for assessing candidates for CO_2 sequestration, *in* M. Grobe, J. C. Pashin, and R. L. Dodge, eds., Carbon dioxide sequestration in geological media — State of the science: AAPG, 297–319.

Peirce, J. W., W. E. Glenn, and K. C. Brown, 1998, High resolution aeromagnetic for hydrocarbon exploration: Canadian Society of Exploration Geophysics Journal, http://www.cseg.ca, accessed 26 April 2010.

Perez, R., O. O. Elebiju, and E. Baruch, 2009, Geophysical evidence of basement controlled faulting in the Ellenburger Group and Viola Limestone, Fort Worth basin, Texas: 79th Annual International Meeting, SEG, Expanded Abstracts, 995–999.

Phillips, J. D., 2007, Geosoft executables (GX's) developed by the U.S. Geological Survey, version 2.0 with notes on GX development from Fortran code: U.S. Geological Survey Open-File Report 2007-1355.

Plotnikova, I. N., 2006, Nonconventional hydrocarbon targets in the crystalline basement, and the problem of recent replenishment of hydrocarbon reserves: Journal of Geochemical Exploration, **89**, 335–338.

Pollastro, R. M., D. M. Jarvie, R. J. Hill, and C. W. Adams, 2007, Geologic framework of the Mississippian Barnett Shale, Barnett-Paleozoic total petroleum system, Bend Arch-Fort Worth basin, Texas: AAPG Bulletin, **91**, 405–436.

Reid, A. B., J. M. Allsop, H. Granser, A.. J. Millett, and I. W. Somerton, 1990, Magnetic interpretation in three dimensions using Euler deconvolution: Geophysics, **55**, 80–91.

Rich, J., 2008, Expanding the applicability of curvature attributes through clarification of ambiguities in derivation and terminology: 78th Annual International Meeting, SEG, Expanded Abstracts, 884–888.

Roest, W. R., J. Verhoef, and M. Pilkington, 1992, Magnetic interpretation using 3-D analytical signal: Geophysics, **57**, 116–125.

Salem, A., S. William, J. D. Fairhead, D. Ravat, and R. Smith, 2007, Tiltdepth method: A simple depth estimation method using first-order derivatives: The Leading Edge, **26**, 1502–1505.

Simon, Y. S., 2005, Stress and fracture characterization in a shale reservoir,

north Texas, using correlation between new seismic attributes and well data: M.S. thesis, University of Houston.

Spaid-Reitz, M. K., and P. M. Eick, 1998, HRAM as a tool for petroleum system analysis and trend exploration: A case study of the Mississippi Delta survey, southeast Louisiana: Canadian Journal of Exploration Geophysics, **34**, 83–96.

Stone, C., 2008, Technology sweeps data from basement: HRAM "flies low" over subtleties: AAPG Explorer, **29**, 22–26.

Sullivan, E. C., K. J. Marfurt, A. Lacazette, and M. Ammerman, 2006, Application of new seismic attributes to collapse chimneys in the Fort Worth basin: Geophysics, **71**, no. 4, B111–B119.

Thomas, W. A., 1989, The Appalachian-Ouachita orogen beneath the Gulf Coastal Plain between the outcrops in the Appalachian and Ouachita Mountains, *in* R. D. Hatcher, W. A. Thomas, and G. W. Viele, eds., The Appalachian-Ouachita orogeny in the United States: Geological Society of America, 537–553.

Thomas, W. A., and D. L. Baars, 1992, A North American continental-scale fracture zone: Workshop on Structural Styles in the Southern Midcontinent, Oklahoma Geological Survey, Abstracts, 3.

Thompson, D. T., 1982, EULDPH: A new technique for making computer-assisted depth estimates from magnetic data: Geophysics, **47**, 31–37.

Verduzco, B., D. J. Fairhead, C. M. Green, and C. MacKenzie, 2004, New insight into magnetic derivatives for structural mapping: The Leading Edge, **23**, 116–119.

Walper, J. L., 1982, Plate tectonic evolution of the Fort Worth basin, *in* C. A. Martin, ed., Petroleum geology of the Forth Worth basin and Bend arch area: Dallas Geological Society, 237–251.

Wilson, F. W., and P. Berendsen, 1998, The role of recurrent tectonics in the formation of the Nemaha uplift and Cherokee-Forest City basins and adjacent structural features in eastern Kansas and contiguous states, USA: Proceedings of 12th International Conference on Basement Tectonics, 301–303.